

## Processing Of Mesoporous Hydroxyapatite Using Cetyltrimethylammonium Bromide (CTAB) As A Porogen And Its Characterization

Nabakumar Pramanik<sup>1\*</sup> and Sudip Chakraborty<sup>2</sup>

<sup>1</sup>Department of Chemistry National Institute of Technology, Arunachal Pradesh-791112, India

<sup>2</sup>Department of Chemistry Indian Institute of Technology, Kharagpur, India

### Abstract

The present research attempt consists in the development of mesoporous hydroxyapatite using inexpensive ingredients using cetyltrimethylammonium bromide (CTAB) as template through a chemical-based hydrothermal method. Wide angle X-ray diffraction (XRD) reveals the formation of pure single-phased hydroxyapatite particles. Fourier transform infrared absorption spectroscopy (FTIR) and electron diffraction X-ray (EDX) studies show the stoichiometric formation of HAp particles. The formation of mesoporous HAp has been confirmed by low angle XRD and Brunauer–Emmett–Teller (BET) surface area analysis studies. Transmission electron microscopy (TEM) analysis divulges needle like acicular crystals of HAp particles with approximate size of 28-36 nm in diameter by 82-94 nm in length. The hemocompatibility study shows that the material is highly hemocompatible. The cell viability study shows that the material is cytocompatible. The developed mesoporous hydroxyapatite material may be used in making a biocomposite, drug delivery and bone tissue engineering applications.

**Keywords:** mesoporous; hydroxyapatite; biomaterials, surface area analysis

### Introduction

During the past decade, much attention has been attracted by mesoporous materials due to their unique surface and textural properties like high surface areas, large and tunable pore size along with large pore volumes, which are crucial for developing new types of catalysts, adsorbents, drug delivery systems, and so on [1]. Since the formation of silicate-based mesoporous material reported in 1992 [2], it has become one of the most energetic research areas of material science. In addition, mesoporous materials have been considered to be excellent candidates for bone reconstruction

## 2. Materials and methods

### 2.1 Chemicals

All chemicals used were of analytical grade and available from commercial sources.

materials due to two major reasons: (i) the porosity and pore volume of biomaterials allow the in-growth of bone tissues to accomplish full integration with the living bones, and deeply promote the formation of bonelike apatite on their surfaces after soaking in simulated body fluids (SBF) [3], and (ii) the mesoporous structure makes it potential to incorporate high dosages of biologically active molecules including osteogenic agents, which can promote bone tissue regeneration and drugs delivery [4].

Hydroxyapatite  $[\text{Ca}_{10}(\text{PO}_4)_6(\text{OH})_2]$  (HAp) is an interesting biomaterial with potential orthopedic, dental and maxillofacial applications because of its excellent biocompatibility, bioactivity and osteoconductivity [5]. In addition, HAp with various morphologies and surface properties has also been explored as drug carriers for delivery of a variety of pharmaceutical molecules owing to its noninflammatory and nontoxic properties [6]. However, a particular attention has been paid to synthesize HAp with porous morphology to favor in-growth of natural bone [7,8]. The increase in surface area resulting from porosity would also contribute to a delivery agent's capacity to adsorb a drug. These porous structures are enormously important for biomedical applications as they have the capability to enhance the adhesion between the bone and the apatite implant.

The present research work describes the development of mesoporous hydroxyapatite. In the full context, we report the synthesis of mesoporous HAp using inexpensive ingredients using cetyltrimethylammonium bromide (CTAB) as porogen template through a chemical-based hydrothermal method. The synthesized materials have been characterized through wide angle X-ray diffraction (XRD), Fourier transform infrared absorption spectroscopy (FTIR), electron diffraction X-ray (EDX), low angle XRD, Brunauer–Emmett–Teller (BET) surface area analysis and transmission electron microscopy (TEM) studies. The biocompatibility has been carried out through hemocompatibility and cell viability studies.

Calcium nitrate (99+%), diammonium hydrogen phosphate (DAHP) (99+%), Cetyltrimethylammonium bromide (CTAB) and

Ammonia solution (25%) were procured from Merck.

## 2.2. Synthesis of mesoporous HAp powders

For the preparation of mesoporous HAp powders, 0.5 (M) stock solution each of calcium nitrate  $[\text{Ca}(\text{NO}_3)_2 \cdot 4\text{H}_2\text{O}]$  and diammonium hydrogen phosphate  $[(\text{NH}_4)_2\text{HPO}_4]$ , DAHP was prepared in deionized water. The two solutions were taken in such amount that Ca:P mole ratio was maintained around 1.67. pH of both the solutions was maintained around 11-12 with the addition of  $\text{NH}_4\text{OH}$  solution. After that CTAB was mixed with DAHP solution ( $\text{PO}_4^{3-}:\text{CTAB}=1:1$  by mole) and allowed to stir for 1h. Subsequently, the CTAB-phosphate solution was added dropwisely to the calcium nitrate solution with vigorous stirring with the help of a magnetic stirrer at room temperature. The pH of the reacting mixture was always maintained around 11-12. A white gelatinous precipitate was obtained. The resulted precipitate was then transferred into a teflon tube (100 ml) held in a stainless steel autoclave, sealed, and maintained at  $150^\circ\text{C}$  for 12 h. As the autoclave cooled to room temperature naturally, the precipitate was separated by filtration, washed with deionized water and ethanol in sequence. Finally, the precipitate was dried keeping it in a vacuum oven at  $90^\circ\text{C}$  over night. The dried precipitate was then grinded by a mortar pestle and calcined at  $600^\circ\text{C}$  for 6 h to remove CTAB.

## 2.3. Characterization

The identification of functional groups in the pure HAp powder and HAp/CTAB samples was analyzed by FTIR analysis (NEXUS870, FTIR, Thermo Nicolet, USA) within the scanning range  $4000$  to  $400\text{ cm}^{-1}$  using KBr technique. The phase analysis of the HAp powder was done by XRD ((Model PW 1729, Philips, Holland) using  $0.67\text{ mA}$ , and  $45\text{ kV}$  current, with a monochromatic  $\text{CuK}\alpha$  (target) radiation ( $\lambda=1.5405\text{ \AA}$ ) with a step size of  $0.05^\circ 2\theta$ , a scan rate of  $0.03^\circ 2\theta/\text{s}$  and a scan range from  $2\theta=20$  to  $60^\circ$ . The XRD technique was also employed to determine the average domain size of the HAp crystals. Small angle XRD patterns were also recorded on the same instrumental system and conditions over the range  $0 \leq 2\theta \leq 8^\circ$ . The morphology, particle size of HAp powder and porosity were observed through a Phillips CM200 transmission electron microscope (TEM) with an acceleration voltage  $100\text{ kV}$ . The textural properties of the synthesized powders were analyzed by the nitrogen adsorption experiment at  $77\text{ K}$  using a surface area analyzer (SA 3100, Beckman Coulter, USA), after degassing the samples at  $90^\circ\text{C}$  for 3 h. Calcium-phosphorous (Ca:P) molar ratio of hydroxyapatite powder was measured by energy dispersive X-ray (EDX) analysis (JEOL, JSM-5800, Japan).

In vitro cytotoxicity study of the material was made by culturing murine fibroblast L929 cells in a contact mode. Briefly, L929 cells were cultured in Dulbecco's modified Eagle's medium (DMEM) and seeded on the sheets/films at their exponential phase of growth at a density of  $10^5\text{ cells/cm}^2$ . The cells were allowed to attach to the films surface for 3 h in  $5\% \text{ CO}_2$  incubator at  $37^\circ\text{C}$ . Fresh DMEM medium supplemented with  $10\%$  fetal calf serum (FCS) was added to each well to maintain the cell containing films submerged. The plates were incubated for 24 h at  $37^\circ\text{C}$  in a humidified atmosphere of  $5\% \text{ CO}_2$  in air. After 24 h incubation, MTT ( $4\text{ mg/ml}$ ) was added to each well at strength of  $10\%$  (v/v) and incubated for further 4 h at  $37^\circ\text{C}$ . Afterward, the media containing MTT was removed and  $200\text{ }\mu\text{l}$  of DMSO was added to dissolve the formazan crystals. The absorbance was measured using an ELISA plate reader (Biorad, USA) at  $595\text{ nm}$ . Student paired *t*-test was performed to test for statistical significance, and a *p*-value of  $<0.05$  was found out to represent a significant difference.

## 3. Results and discussion

The FTIR spectra of HAp/CTAB system and calcined HAp are shown in Fig. 1. The IR bands at  $3572$  and  $632\text{ cm}^{-1}$  belong to the vibration of structural-OH groups of hydroxyapatite. The bands at  $1093$  ( $\gamma_3, \text{PO}_4^{3-}$ ),  $1036$  ( $\gamma_3, \text{PO}_4^{3-}$ ), and  $962$  ( $\gamma_1, \text{PO}_4^{3-}$ ),  $\text{cm}^{-1}$  are characteristic of the phosphate stretching vibration, and the bands observed at  $602$  ( $\gamma_4, \text{PO}_4^{3-}$ ),  $565$  ( $\gamma_4, \text{PO}_4^{3-}$ ), and  $472$  ( $\gamma_2, \text{PO}_4^{3-}$ )  $\text{cm}^{-1}$  are due to the phosphate bending vibration (Fig. 1a) [9].

Some carbonate anion derived bands are also observed at  $1456$  and  $1408\text{ cm}^{-1}$ , resulting from the dissolved  $\text{CO}_2$  from the atmosphere during mixing, stirring and material precipitation. The strong absorption bands at  $2954$  and  $2848\text{ cm}^{-1}$  are assigned to C-H stretch of  $\text{CH}_3$ -,  $-\text{CH}_2$ - of CTAB (Fig. 1a) [10]. After calcination, the strong bands at  $2954$  and  $2848\text{ cm}^{-1}$  have vanished (Fig. 1b), implying no residual CTAB species in the calcined sample is present. This phenomenon indicates that using calcination method, the CTAB templates in HAp solid can be removed completely.

The X-ray diffraction pattern of the calcined apatite powder has been presented in Fig. 2. The *d*-values correspond to that of hexagonal calcium hydroxyapatite with space group  $\text{P6}_3/\text{m}$   $[\text{Ca}_{10}(\text{PO}_4)_6(\text{OH})_2]$  (JCPDS card no. 09-0432). The broadening of XRD peaks indicates nanocrystalline nature of the synthesized apatite powders. It is evident from the observed results that no characteristic diffraction angles from other calcium phosphate phases are detected. The main crystalline peaks observed for the pure HAp at diffraction angles  $25.89^\circ$ ,  $31.91^\circ$ ,  $32.95^\circ$ ,  $34.08^\circ$ ,  $39.85^\circ$ , and

46.71° respectively represent the hydroxyapatite phase with d-spacing 3.44, 2.80, 2.72, 2.63, 2.26, and 1.94 Å correspondingly. The mean domain size has been calculated using Scherrer's equation i.e.

$$D = \frac{0.9\lambda}{\beta \cos \theta}$$

where D is the average domain size in Å,  $\beta$  is the peak broadening of the diffraction line measured at half of its maximum intensity in "radian",  $\lambda$  is the wavelength of X-rays, and  $\theta$  is the Bragg's diffraction angle. The average domain size for the calcined HAp powder is found to be 38 nm. The relationship between lattice constant (a & c), Miller's indices (h,k,l) and lattice spacing (d) is used to calculate lattice parameter values i.e.

$$\frac{1}{d^2} = \frac{4}{3} \left( \frac{h^2 + hk + k^2}{a^2} \right) + \frac{l^2}{c^2}$$

The lattice parameters are found to be a=b=9.42 Å and c=6.88 Å. Therefore, the wide angle XRD reveals that the synthesized calcined material is pure hydroxyapatite phase, which is supported by the result raised from FTIR analysis also. The result is also supported by the energy dispersive X-ray analysis (EDX), which indicates the material is stoichiometric with Ca: P mole ratio 1.66 (theoretical value 1.67).

Figure 3 shows low angle X-ray diffraction (XRD) pattern of HAp powders calcined at 600°C. A single sharp low angle diffraction peak [100] has been appeared at 2 $\theta$  value around 1.57°, which corresponds to the d-spacing value of 5.28 nm. The atomic plane may have resulted from pores generated in the materials. The reflection peaks at low angle region do not allow structural assignment of the sample, but the low angle diffraction peak generally appears due to presence of mesostructural nature of the sample [11].

The textural property of the calcinated material has been investigated through BET surface area analysis. Fig. 4 is the nitrogen adsorption and desorption isotherms of calcined HAp powders, which exhibit a mesoporous materials type IV isotherm under BDDT (Brunauer-Deming-Deming-Teller) system (IUPAC) with typical H1 hysteresis loop according to IUPAC classification, and a well-defined step at approximately P/P<sub>0</sub> = 0.83–0.97, implying the mesostructural nature of the material. Besides, based on overall investigation on the N<sub>2</sub> adsorption–desorption data, the specific surface area and pore volume of mesoporous HAp are found to be 56 m<sup>2</sup>/g and 0.24 cm<sup>3</sup>/g respectively.

The morphology, particle size and pores have been investigated through TEM analysis. Fig. 5 shows the TEM micrograph of calcinated HAp

powders. The micrograph depicts needle like acicular crystals of HAp particles with approximate size of 28-36 nm in diameter by 82-94 nm in length. The existence of pores and their disordered arrangement were displayed in the Figure. Although it was not possible to calculate the exact pore size from the TEM image due to the low resolution of TEM technique, the approximate diameter of the pores is found to be 4-5 nm. This suggests that the pores are generated through the imprinting of the individual CTAB molecule in the synthesized material.

The hemocompatibility test is mainly aimed to find out the extent of hemolysis caused in the presence of the samples i.e. hemolysis indicates premature damage of red blood cells when they come in contact with the samples. When the hemolysis percentage is less than 10, the test material is considered as hemocompatible and if it is less than 5, the material is taken as highly hemocompatible [12]. The percentage of hemolysis obtained for the hydroxyapatite material is calculated to be 1.94. Therefore, the results show that the material is highly hemocompatible.

The in vitro cytotoxicity of the hydroxyapatite sample has been investigated through MTT assay test. A cell line of murine fibroblast (L929) has been selected for this test. The difference in cell viability index is shown in Fig. 6 of the composite samples of different concentrations, as compared to the control tissue culture plate. The statistical analysis (student's t-test) has indicated that the difference in cell viability index is insignificant. Hence, the developed hydroxyapatite material is cytocompatible.

#### 4. Conclusion

A successful manifestation on formation of mesoporous hydroxyapatite has been presented here. XRD study confirms that the synthesized material restrains single phase pure hydroxyapatite. EDX study shows that the material is stoichiometric with Ca:P mole ratio of 1.66. Low angle XRD analysis confirms that the HAp product is mesostructured in nature. This result is in well consistent with the BET result, which also confirms that the material is mesoporous in nature with specific surface area 56 m<sup>2</sup>/g and pore volume 0.24 cm<sup>3</sup>/g. TEM analysis the morphology of Hap powders with dimensions of 28-36 nm in diameter by 82-94 nm in length and also shows the presence of pores and their disordered arrangement with approximate pore size 4-5 nm. The developed mesoporous hydroxyapatite material may have applications in making a biocomposite, drug delivery and bone tissue reconstruction engineering.

### Acknowledgement

Authors are thankful to IIT Kharagpur for support.

### References

- [1] A. Dong, N. Ren, Y. Tang, Y. Wang, Y. Zhang, W. Hua, and Z. Gao, "General synthesis of mesoporous spheres of metal oxides and phosphates," J Am Chem Soc, 2003; vol. 125: pp. 4976-4977.
- [2] C. T. Kresge, M. E. Leonowicz, and W. J. Roth, "Ordered mesoporous molecular sieves synthesized by a liquid-crystal template mechanism," Nature, 1992; vol. 359: pp. 710-712.
- [3] Y. P. Guo, Y. Zhou, and D. C. Jia, "Fabrication of hydroxycarbonate apatite coatings with hierarchically porous structures," Acta Biomater, 2008; vol. 4: pp. 334-342.
- [4] X. T. Shi, Y. J. Wang, L. Ren, N. R. Zhao, Y. H. Gong, and D. A. Wang, "Novel mesoporous silica-based antibiotic releasing scaffold for bone repair," Acta Biomater, 2009; vol. 5: pp. 1697-1707.
- [5] K. S. Vecchio, X. Zhang, J. B. Massie, M. Wang, and C. W. Kim, "Conversion of bulk seashells to biocompatible hydroxyapatite for bone implants," Acta Biomater, 2007; vol. 3: pp. 910-918.
- [6] A. Almirall, G. Larrecq, and J. A. A. Delgado, "Fabrication of low temperature macroporous hydroxyapatite scaffolds by foaming and hydrolysis of an  $\alpha$ -TCP paste," Biomaterials, 2004; vol. 17: pp. 3671-3680.
- [7] T. Brendel, A. Engel, and C. Rüssel, "Hydroxyapatite coatings by a polymeric route," J Mater Sci Mater Med, 1992; vol. 3: pp. 175-179.
- [8] D. Walsh, T. Furuzono, and J. Tanaka, "Preparation of porous composite implant materials by in situ polymerization of porous apatite containing  $\epsilon$ -caprolactone or methyl methacrylate," Biomaterials, 2001; vol. 22: pp. 1205-1212.
- [9] A. Lak, M. Mazloumi, M. Mohajerani, A. Kajbafvala, S. Zanganeh, H. Arami, and S. K. Sadrnezhad, "Self-assembly of dandelionlike hydroxyapatite nanostructures via hydrothermal method," J Am Ceram Soc, 2008; vol. 91: pp. 3292-3297.
- [10] L. Yanbao, T. Wiliana, and K. C. Tam, "Synthesis and characterization of nanoporous hydroxyapatite using cationic surfactants as templates," Mater Res Bull, 2008; vol. 43: pp. 2318-2326.
- [11] M. Tiemann and M. Froeba, "Mesoporous aluminophosphates from a single-source precursor," Chem Commun, 2002; pp. 406-407.
- [12] S. K. Ray Chowdhury, A. Mishra, B. Pradhan and D. Saha, "Wear characteristic and biocompatibility of some polymer composite acetabular cups," Wear, 2004; vol. 256: pp. 1026-1036.

Fig. 1

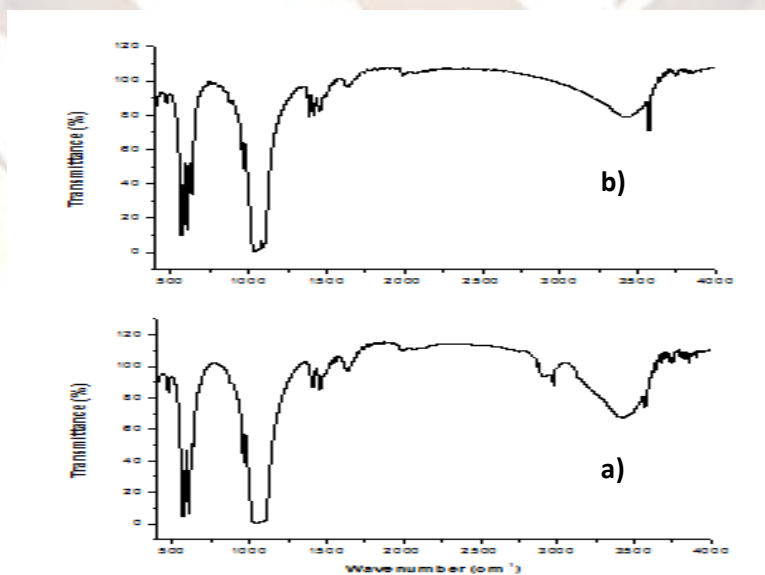


Fig. 1 FTIR spectra of a) as synthesized HAP with CTAB b) calcined HAP.

Fig. 2

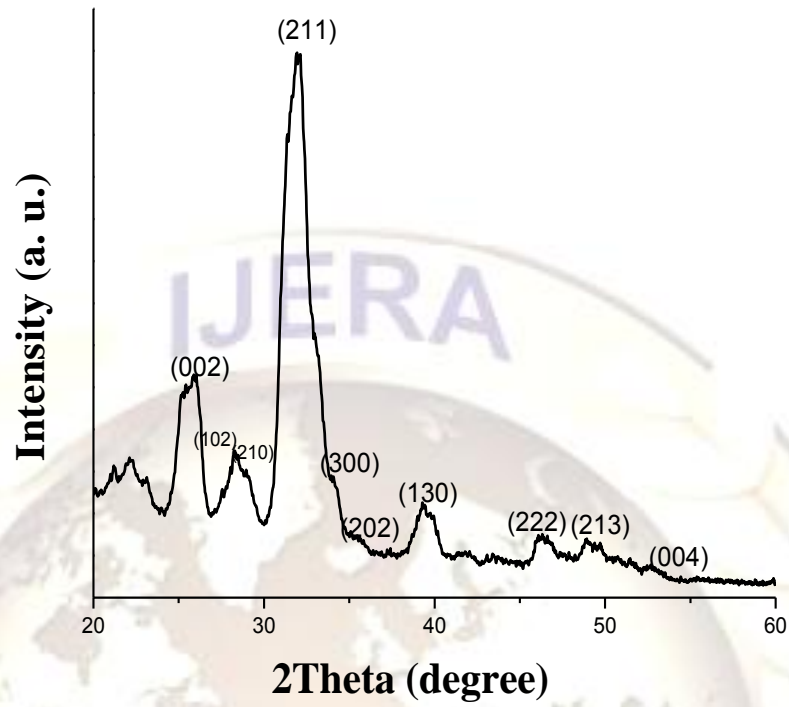


Fig. 2 XRD pattern of calcined HAp powders.

Fig. 3

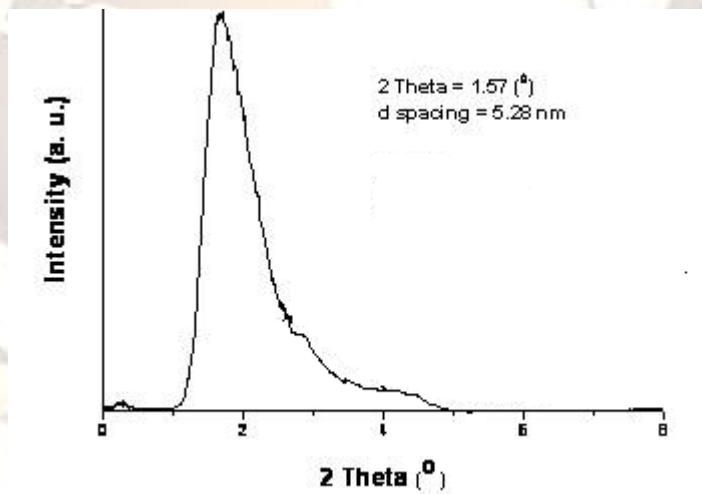


Fig. 3 Low angle XRD of calcined HAp powders.

Fig. 4

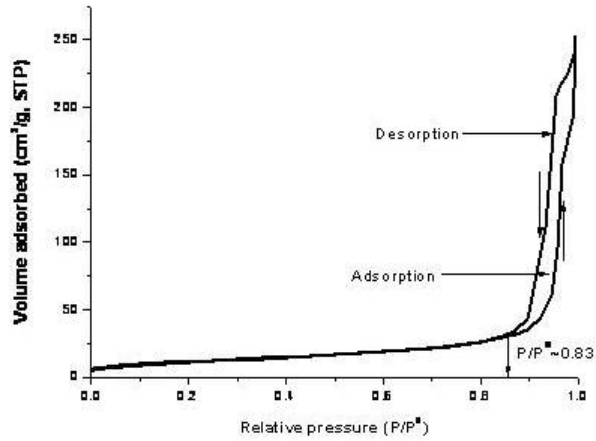


Fig. 4 BET N<sub>2</sub> adsorption/desorption isotherms of calcined HAp powders.

Fig. 5

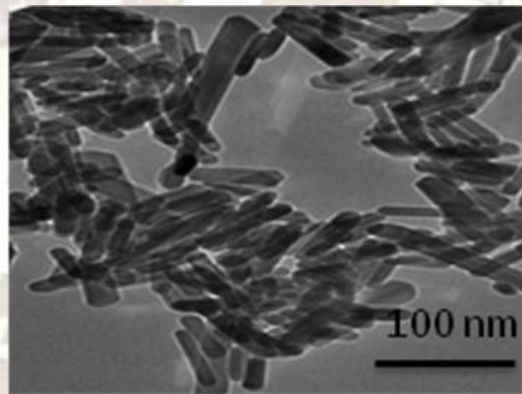


Fig. 5 TEM micrograph of calcined HAp.

Fig. 6

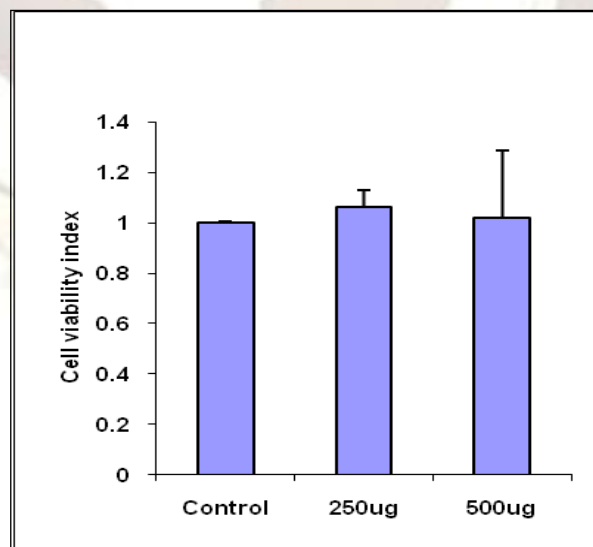


Fig. 6 The MTT assay of cells (L929) cultured on composite samples with different concentrations.